The Astrophysical Journal, 587:714–726, 2003 April 20

RESOLUTION OF DISTANCE AMBIGUITIES OF INNER GALAXY MASSIVE STAR FORMATION REGIONS. I.

C. Watson,[1] E. Araya,[2] M. Sewilo,[1] E. Churchwell,[1] P. Hofner,[2,3] and S. Kurtz[4]

Received 2002 October 30; accepted 2002 December 18

ABSTRACT

Fifty-four ultracompact (UC) H II regions in the GLIMPSE survey region ($|b| < 1^\circ$ and $30^\circ < l < 70^\circ$) were observed in H_2CO and H110α using the 305 m Arecibo telescope. By analyzing H_2CO absorption against the UC H II region continuum emission, we resolve the distance ambiguity toward 44 sources. This determination is critical to measure global physical properties of UC H II regions (e.g., luminosity, size, mass) and properties of the Galaxy (e.g., spiral structure, abundance gradients). We find that the distribution of UC H II regions in this survey is consistent with a "local spur," the Perseus, Sagittarius, and Scutum arms as delineated by Taylor & Cordes. However, departures from model velocities produce distance uncertainties only slightly smaller than the proposed arm separations.

Subject headings: Galaxy: disk — radio lines: general — stars: formation

On-line material: machine-readable tables

1. INTRODUCTION

Accurate distances are essential to trace global properties of the Galaxy, such as the spiral structure of the Milky Way, abundance gradients, and other parameters that depend on Galactocentric radius. The physical properties of individual objects such as size, luminosity, and mass also depend on independent distance determinations. The distances to almost all ultracompact (UC) H II regions (massive star formation regions) are kinematic distances because they are too heavily obscured to use any of the optical distance determination techniques. Kinematic distances depend on a rotation model of the Galaxy. An error in the derived distance occurs when the actual velocity of an object departs from that assumed in the model. These are designated peculiar motions and are typically $\lesssim 10$ km s^{-1} (Bania & Lockman 1984), but a few examples are known to exceed this value. Peculiar motions can cause distance uncertainties of a few hundred pc to $\sim$2 kpc, depending on the location of the source. In the inner Galaxy (i.e., interior to the solar circle), a distance ambiguity exists because along each line of sight a circular orbit of radius smaller than that of the Sun will intersect the line of sight at two points, designated the near and far distances. At the two intersection points an object has the same radial velocity; consequently, one cannot distinguish between the near and far distance.

The main goal of this paper is to resolve the distance ambiguity of as many massive star formation regions within the Galactic longitude $l = 32^\circ$–70° and Galactic latitude $|b| \leq 1^\circ$ as possible. We use UC H II regions as a tracer of massive star formation regions. The motivations for this program are to (1) provide distances to massive star formation regions for the *SIRTF*/GLIMPSE survey of the inner Galax, (2) provide a more accurate basis for deriving physical properties of H II regions and their associated massive star formation regions, and (3) compare the distribution of UC H II regions with the best recent determination of spiral arms in the inner Galaxy. Because of their extreme youth, UC H II regions should be an excellent tracer of spiral arms. However, as noted by Kurtz, Churchwell, & Wood (1994), distance errors confuse spiral arms traced by UC H II regions except possibly the local spur. There is considerable uncertainty about both the number and location of the spiral arms in the Milky Way. A summary by Vallee (1995) of the papers reporting spiral arm structure in the Galaxy since 1980 lists 15 models claiming two, three, and four spiral arms. Vallee (1995) suggested that the weight of the data favors a 4 arm logarithmic spiral pattern.

In the first paper of this study, Araya et al. (2002) observed 21 UC H II regions in the H110α and H_2CO (1_{11}–1_{01}) lines using the Arecibo 305 m telescope with a resolution of 1′. The H110α line was used to establish the radial velocity of the H II region, and the H_2CO absorption line was used to resolve the distance ambiguity. Of the 21 sources observed, the distance ambiguity was resolved for 20 sources. Fish et al. (2003) used the Very Large Array (VLA) to observe the H I 21 cm line in absorption toward 20 UC H II regions and successfully resolved the distance ambiguity for each of them. In this paper, we continue the efforts of (Araya et al. 2002) and present further observations of H110α emission and H_2CO (1_{11}-1_{10}) absorption lines using the Arecibo 305 m telescope. We observed 54 UC H II region candidates to extend the list of well-resolved distance ambiguities. We examine evidence for spiral structure based on all UC H II regions for which distance ambiguities have been resolved with spatial resolutions $\leq 1'$.

2. OBSERVATIONS

We selected sources from the *IRAS* Point Source catalog that (1) satisfy the far-infrared point-source color-color criteria for UC H II regions [i.e., $\log(S_{60\,\mu m}/S_{12\,\mu m}) \geq 1.30$ and $\log(S_{25\,\mu m}/S_{12\,\mu m}) \geq 0.57$; Wood & Churchwell 1989], (2) have 100 μm flux density $\geq$700 Jy, and (3) are visible from

[1] University of Wisconsin, Madison, Department of Astronomy, 475 North Charter Street, Madison, WI 53716.
[2] University of Puerto Rico at Rio Piedras, Physics Department, P.O. Box 23343, San Juan, PR 00931.
[3] Arecibo Observatory, NAIC/Cornell University, HC3 Box 53995, Arecibo, PR 00612.
[4] Instituto de Astronomia, UNAM, Apartado Postal 70-264, Mexico, DF, 04510, Mexico.

Arecibo with the 305 m Telescope and lie within the *SIRTF*/GLIMPSE survey region ($|l| = 10°$–$70°$ and $|b| \leq 1$). The sources are given in Table 1. The goal is to establish reliable distances to OB associations and clusters that lie within the *SIRTF*/GLIMPSE survey. The survey reported here is the second of four that will be required to cover the *SIRTF*/GLIMPSE survey area.

TABLE 1
OBSERVED SOURCES

Source	α(B1950)	δ(B1950)	*IRAS* Name	$S_{100\,\mu m}$ ($\times 10^2$ Jy)
G32.11+0.09.....	18 47 02.1	−00 44 35	18470−0044	12.0
G32.15+0.13.....	18 46 59.6	−00 41 30	18469−0041	8.1
G32.99+0.04.....	18 48 51.1	00 00 41	18488+0000	9.2
G33.20−0.01.....	18 49 24.0	00 10 31	18494+0010	21.8
G33.24+0.01.....	18 49 24.4	01 13 20	18494+0113	7.2
G33.29−0.02.....	18 49 35.6	00 14 48	18495+0014	21.8
G33.81−0.19.....	18 51 09.1	00 38 00	18511+0038	12.9
G34.09+0.44.....	18 49 27.1	01 10 02	18494+0110	7.2
G34.40+0.23.....	18 50 45.2	01 21 09	18507+0121	19.5
G35.03+0.34.....	18 51 32.7	01 57 45	18515+0157	33.0
G35.04−0.50.....	18 54 34.6	01 34 49	18545+0134	14.9
G35.47+0.14.....	18 53 03.0	02 15 13	18530+0215	19.2
G35.58−0.03.....	18 53 52.3	02 16 39	18538+0216	25.9
G35.67−0.04.....	18 54 04.5	02 20 54	18540+0220	8.3
G36.40+0.02.....	18 55 11.8	03 02 00	18551+0302	8.0
G37.20−0.43.....	18 58 16.1	03 31 40	18582+0331	6.2
G37.37−0.24.....	18 57 54.0	03 45 56	18578+0345	17.2
G37.54−0.11.....	18 57 46.5	03 58 52	18577+0358	18.7
G37.75−0.10.....	18 58 07.3	04 09 58	18581+0409A	8.8
G37.76−0.20.....	18 58 30.2	04 07 48	18585+0407	21.5
G39.25−0.07.....	19 00 48.0	05 30 52	19008+0530	17.1
G39.39−0.14.....	19 01 17.7	05 36 10	19012+0536	8.3
G40.42+0.70.....	19 00 13.5	06 54 37	19002+0654	7.1
G40.62−0.14.....	19 03 34.9	06 41 55	19035+0641	9.2
G42.11−0.44.....	19 07 28.4	07 52 26	19074+0752	7.6
G42.43−0.26.....	19 07 25.6	08 14 44	19074+0814	21.0
G43.17+0.00.....	19 07 51.7	09 01 11	19078+0901	362.
G43.18−0.52.....	19 09 46.3	08 47 09	19097+0847	14.5
G43.24−0.05.....	19 08 11.4	09 03 22	19081+0903	22.5
G43.26−0.21.....	19 08 42.1	09 00 05	19087+0900	6.7
G43.79−0.12.....	19 09 30.2	09 30 42	19095+0930	27.4
G45.48+0.18.....	19 11 47.3	11 07 13	19117+1107	78.9
G45.82−0.29.....	19 13 57.2	11 13 47	19139+1113	12.9
G45.93−0.40.....	19 14 34.5	11 16 20	19145+1116	8.7
G48.63+0.23.....	19 17 31.0	13 57 09	19175+1357	11.5
G49.21−0.35.....	19 20 44.6	14 10 50	19207+1410	74.5
G49.67−0.45.....	19 22 02.2	14 32 07	19220+1432	17.5
G50.28−0.39.....	19 23 00.9	15 06 28	19230+1506	13.7
G50.31+0.67.....	19 19 11.0	15 38 13	19191+1538	5.8
G51.68+0.72.....	19 21 44.0	16 51 43	19217+1651	6.6
G52.23+0.74.....	19 22 45.8	17 21 35	19227+1721	15.4
G53.03+0.12.....	19 26 40.1	17 45 41	19266+1745	5.7
G53.63+0.02.....	19 28 14.7	18 14 32	19282+1814	22.8
G54.09−0.06.....	19 29 29.8	18 36 07	19294+1836	21.4
G57.55−0.27.....	19 37 30.2	21 30 30	19375+2130	9.2
G58.77+0.65.....	19 36 40.1	23 01 43	19366+2301	7.0
G59.14−0.11.....	19 40 19.8	22 58 06	19403+2258	6.4
G59.36−0.21.....	19 41 10.1	23 06 47	19411+2306	5.8
G59.60+0.92.....	19 37 26.4	23 52 57	19374+2352	7.7
G59.76−0.03.....	19 41 21.5	23 32 51	19413+2332	16.3
G59.78+0.06.....	19 41 04.2	23 36 54	19410+2336	16.3
G63.05−0.34.....	19 49 55.7	26 13 25	19499+2613	3.2
G63.12+0.44.....	19 47 06.1	26 41 16	19471+2641	16.7
G69.54−0.98.....	20 08 09.9	31 22 39	20081+3122	31.2

NOTE.—Units of right ascension are hours, minutes, and seconds, and units of declination are degrees, arcminutes, and arcseconds.

The observations were made between 2002 July 24 and 29 with the 305 m Arecibo Telescope. The 1_{10}–1_{11} transition of interstellar formaldehyde (H_2CO, $\nu_o = 4829.6594$ MHz for $F = 2$–2) was observed in absorption against UC H II regions. Simultaneously, the H110α ($\nu_o = 4874.1570$ MHz) radio recombination line was observed to establish kinematic distances.

Both H_2CO and H110α line transitions were observed using the Gregorian *C*-band receiver. The beamwidth of the Arecibo telescope at 4.86 GHz was measured to be $0'.95 \pm 0'.02$. Four independent correlator boards were used to measure both spectral lines simultaneously in both senses of linear polarization; 2048 channels per subcorrelator and nine-level sampling were used. A total bandwidth of 6.25 and 12.5 MHz was used resulting in resolutions of 3.05 kHz (0.19 km s^{-1}) and 6.10 kHz (0.38 km s^{-1}), and total velocity coverages of $\sim$390 and $\sim$770 km s^{-1} for H_2CO and H110α, respectively. The central velocity for all spectra was set to $V_{LSR} = 0$ km s^{-1}.

Position switching was used with 5 minutes spent on both the "on" and "off" positions, followed by 10 s integrations at the off position with and without a noise-diode calibration signal. The off position was chosen to trace the same path on the sky as the on-source position. A few sources required 10–15 minutes on-source integration time to achieve a signal-to-noise ratio (S/N) $\geq$10. For both polarizations, the system temperature during the observations was $\sim$35 K. A typical rms was 1 mJy. From observations of flux calibrators, the antenna gains varied between 7.8 and 9.1 K Jy^{-1} as a function of zenith and azimuth angles. Flux calibration is accurate to $\sim$15% based on antenna gain variation at a given zenith angle. Line intensities of individual scans were corrected for gain variation with zenith angle. For each source both on and off positions were inspected individually to check for absorption and/or emission in the off position and for radio interference. The final spectra were obtained by averaging both polarizations and all scans for a particular source.

3. RESULTS

The spectral lines were analyzed using the CLASS software package.[5] Gaussian profiles were fitted to both the H110α and H_2CO lines. For H_2CO, a Gaussian was fitted to each velocity component along the line of sight. Non-Gaussian components were observed in seven sources (G32.99+0.04, G33.29−0.02, G35.58−0.03, G37.54−0.11, G43.17+0.00, G50.28−0.39, G51.68+0.72). Continuum emission was detected in most cases and measured from both the H110α and H_2CO spectra. The line parameters for H110α and H_2CO transitions and related continuum measurements are presented in Tables 2 and 3, respectively. The errors quoted in the tables are the formal 1 σ errors (68.3% confidence level) of the Gaussian fits to the data. The detection threshold is 3 σ. Both H_2CO and H110α spectral lines for individual sources are presented in Figure 1.

We observed 54 sources, 44 of which were detected in H110α emission and 54 of which were detected in H_2CO absorption. To calculate the kinematic distance, we make

[5] CLASS is part of the GILDAS software developed by IRAM.

TABLE 2

H110α Line and Continuum Parameters

Source	S_c (mJy)	$S_{H110\alpha}$ (mJy)	V_{LSR} (km s^{-1})	FWHM (km s^{-1})	$\int S_v\,dv$ (mJy km s^{-1})
G32.11+0.09.....	62.9 (0.7)	3.5 (0.7)	93.0 (1.5)	22.7 (4.7)	85 (10)
G32.15+0.13.....	533.8 (1.4)	33.9 (1.4)	95.0 (0.2)	25.6 (0.6)	922 (20)
G32.99+0.04.....	213.7 (0.9)	11.6 (0.9)	89.0 (0.6)	23.7 (1.5)	293 (10)
G33.20−0.01.....	285.6 (0.9)	21.4 (0.9)	105.8 (0.3)	23.5 (0.7)	535 (10)
G33.24+0.01.....	461.8 (1.1)	25.5 (1.1)	35.1 (0.3)	26.2 (0.7)	712 (10)
G33.29−0.02.....	43.0 (0.5)	...	...	...	...
G33.81−0.19.....	145.8 (1.5)	12.2 (1.5)	40.3 (0.6)	22.4 (1.5)	291 (20)
G34.09+0.44.....	178.8 (0.9)	11.1 (0.9)	32.6 (0.5)	21.8 (1.2)	258 (10)
G34.40+0.23.....	62.8 (0.7)	5.0 (0.7)	60.1 (1.3)	16.9 (6.0)	90 (20)
G35.03+0.34.....	39.9 (1.1)	3.7 (1.1)	57.2 (1.4)	20.9 (3.0)	83 (10)
G35.04−0.50.....	310.5 (0.9)	16.7 (0.9)	48.0 (0.4)	25.9 (0.9)	460 (10)
G35.47+0.14.....	224.8 (1.7)	18.1 (1.7)	80.9 (0.5)	28.6 (1.4)	552 (20)
G35.58−0.03.....	461.6 (0.7)	20.0 (0.7)	52.5 (0.3)	29.7 (0.7)	633 (10)
G35.67−0.04.....	395.4 (1.6)	16.8 (1.6)	51.9 (0.7)	34.9 (1.8)	625 (30)
G36.40+0.02.....	83.1 (0.7)	3.7 (0.7)	53.3 (1.4)	22.3 (3.3)	88 (10)
G37.20−0.43.....	123.5 (0.8)	9.1 (0.8)	38.0 (0.5)	20.4 (1.2)	198 (10)
G37.37−0.24.....	258.0 (0.9)	15.1 (0.9)	39.4 (0.4)	25.2 (1.1)	403 (10)
G37.54−0.11.....	765.1 (1.1)	36.9 (1.1)	48.9 (0.2)	30.0 (0.5)	1180 (20)
G37.75−0.10.....	367.0 (1.1)	23.0 (1.1)	49.7 (0.3)	23.1 (0.7)	566 (20)
G37.76−0.20.....	1196.7 (1.0)	70.5 (1.0)	66.6 (0.1)	25.4 (0.4)	1900 (20)
G39.25−0.07.....	668.8 (1.3)	36.4 (1.3)	23.0 (0.2)	25.0 (0.5)	969 (20)
G39.39−0.14.....	43.4 (0.4)	...	...	...	...
G40.42+0.70.....	66.9 (0.6)	5.2 (0.6)	20.1 (0.8)	20.1 (1.8)	111 (10)
G40.62−0.14.....	−50.3 (0.9)	...	...	...	...
G42.11−0.44.....	196.2 (1.1)	11.2 (1.1)	53.4 (0.6)	29.0 (1.3)	344 (10)
G42.43−0.26.....	562.9 (1.2)	20.2 (1.2)	61.5 (0.4)	38.5 (1.0)	827 (20)
G43.17+0.00.....	13956.0 (5.7)	647.0 (5.7)	7.4 (0.3)	32.3 (0.7)	22200 (420)
G43.18−0.52.....	514.6 (0.9)	35.3 (0.9)	59.1 (0.2)	23.0 (0.4)	863 (10)
G43.24−0.05.....	788.7 (1.4)	39.7 (1.4)	9.4 (0.2)	25.2 (0.5)	1060 (20)
G43.26−0.21[a]	1666.2 (1.2)	...	...	...	...
G43.79−0.12.....	108.8 (0.5)	4.1 (0.5)	43.3 (1.1)	31.9 (3.0)	141 (10)
G45.48+0.18.....	1349.5 (1.3)	71.0 (1.3)	55.6 (0.1)	29.5 (0.3)	2230 (20)
G45.82−0.29.....	432.0 (0.7)	24.1 (0.7)	61.2 (0.2)	26.3 (0.5)	676 (10)
G45.93−0.40.....	113.9 (0.7)	9.4 (0.7)	63.9 (0.5)	21.1 (1.3)	212 (10)
G48.63+0.23.....	229.1 (1.0)	14.7 (1.0)	9.4 (0.4)	23.1 (0.9)	360 (10)
G49.21−0.35.....	3335.2 (1.3)	168.0 (1.3)	68.1 (0.1)	27.9 (0.4)	4990 (50)
G49.67−0.45.....	75.7 (0.7)	3.2 (0.7)	62.7 (1.6)	38.3 (3.1)	132 (10)
G50.28−0.39.....	274.9 (0.6)	17.3 (0.6)	10.3 (0.3)	23.9 (0.7)	440 (10)
G50.31+0.67.....	171.8 (0.8)	10.4 (0.8)	25.9 (0.5)	23.4 (1.1)	260 (10)
G51.68+0.72.....	−8.6 (0.9)	...	...	...	...
G52.23+0.74.....	238.2 (0.8)	19.6 (0.8)	−3.0 (0.4)	21.4 (1.0)	446 (20)
G53.03+0.12.....	27.4 (1.0)	...	...	...	...
G53.63+0.02.....	44.9 (0.6)	1.9 (0.6)	31.2 (2.2)	31.9 (4.7)	65 (10)
G54.09−0.06.....	337.1 (0.6)	24.3 (0.6)	42.8 (0.2)	20.8 (0.4)	536 (10)
G57.55−0.27.....	240.0 (0.6)	12.6 (0.6)	6.3 (0.3)	25.9 (0.7)	346 (10)
G58.77+0.65.....	46.1 (0.6)	3.1 (0.6)	30.0 (1.1)	22.8 (2.6)	75 (10)
G59.14−0.11.....	8.0 (0.9)	...	...	...	...
G59.36−0.21.....	30.1 (0.3)	1.9 (0.3)	26.6 (1.6)	29.5 (5.1)	60 (10)
G59.60+0.92.....	49.8 (0.7)	1.4 (0.7)	46.4 (2.1)	21.6 (5.4)	32 (<10)
G59.76−0.03.....	13.7 (0.8)	...	...	...	...
G59.78+0.06.....	2.9 (0.7)	...	...	...	...
G63.05−0.34.....	42.2 (1.2)	3.1 (1.2)	−9.3 (2.3)	22.8 (8.8)	76 (20)
G63.12+0.44.....	212.7 (0.9)	13.2 (0.9)	16.4 (0.4)	22.1 (1.0)	311 (10)
G69.54−0.98.....	37.1 (0.9)	...	...	...	...

Note.—Table 2 is also available in machine-readable form in the electronic edition of the *Astrophysical Journal*.

[a] This source is a supernova remnant (see Brogan & Troland 2001).

TABLE 3

H_2CO Line Parameters

Source Direction[a]	S_c (mJy)	S_{H_2CO} (mJy)	V_{LSR} (km s^{-1})	FWHM (km s^{-1})	$\int S_v\, dv$ (mJy km s^{-1})
G32.11+0.09 MC1	64.5 (1.6)	−6.9 (1.6)	9.3 (0.2)	1.9 (0.4)	−14 (<10)
G32.11+0.09 MC2		−26.5 (1.6)	96.1 (0.1)	3.2 (0.2)	−91 (<10)
G32.15+0.13 MC1	544.4 (2.1)	−12.4 (2.1)	10.3 (0.5)	2.0 (2.0)	−27 (20)
G32.15+0.13 MC2		−105.0 (2.1)	94.2 (0.1)	4.0 (0.2)	−444 (20)
G32.99+0.04 MC1	216.8 (2.0)	−8.6 (2.0)	10.3 (0.5)	3.0 (1.1)	−28 (10)
G32.99+0.04 MC2		−32.0 (2.0)	83.0 (0.1)	3.6 (0.5)	−123 (10)
G32.99+0.04 MC3		−34.4 (2.0)	99.0 (0.1)	2.7 (0.4)	−99 (10)
G32.99+0.04 MC4		−51.0 (2.0)	104.6 (0.1)	2.1 (0.2)	−115 (10)
G32.99+0.04 MC5		−8.3 (2.0)	141.8 (0.4)	1.1 (0.8)	−10 (10)
G33.20−0.01 MC1	292.1 (2.0)	−23.6 (2.0)	10.5 (0.1)	1.7 (0.2)	−42 (<10)
G33.20−0.01 MC2		−12.7 (2.0)	74.5 (0.2)	3.3 (0.5)	−45 (10)
G33.20−0.01 MC3		−50.5 (2.0)	98.9 (0.1)	3.7 (0.1)	−199 (10)
G33.24+0.01 MC1	465.1 (2.2)	−10.3 (2.2)	13.6 (0.8)	2.9 (2.2)	−32 (20)
G33.24+0.01 MC2		−35.2 (2.2)	33.6 (0.2)	2.8 (0.5)	−103 (20)
G33.24+0.01 MC3		−14.6 (2.2)	57.5 (0.5)	2.7 (1.3)	−42 (20)
G33.24+0.01 MC4		−10.9 (2.2)	89.4 (0.7)	2.1 (1.7)	−24 (20)
G33.29−0.02 MC1	44.2 (1.2)	−32.8 (1.2)	99.8 (0.1)	3.2 (0.1)	−111 (<10)
G33.81−0.19 MC1	150.8 (2.5)	−16.7 (2.5)	11.3 (0.1)	0.9 (0.9)	−15 (<10)
G33.81−0.19 MC2		−29.9 (2.5)	50.5 (0.2)	5.8 (0.7)	−185 (10)
G33.81−0.19 MC3		−9.8 (2.5)	78.4 (0.3)	2.4 (0.6)	−25 (10)
G33.81−0.19 MC4		−10.1 (2.5)	87.6 (0.2)	1.5 (0.5)	−17 (<10)
G34.09+0.44 MC1	180.1 (2.1)	−10.3 (2.1)	34.0 (0.4)	3.8 (0.9)	−42 (10)
G34.40+0.23 MC1	64.1 (1.9)	−66.9 (1.9)	57.2 (< 0.1)	5.4 (0.1)	−383 (10)
G35.03+0.34 MC1	40.9 (2.0)	−10.4 (2.0)	14.1 (0.2)	2.3 (0.5)	−26 (<10)
G35.03+0.34 MC2		−9.3 (2.0)	43.1 (0.2)	3.6 (0.5)	−36 (<10)
G35.03+0.34 MC3		−26.0 (2.0)	51.9 (0.1)	3.8 (0.2)	−107 (<10)
G35.03+0.34 MC4		−8.5 (2.0)	92.6 (0.2)	2.3 (0.4)	−21 (<10)
G35.04−0.50 MC1	311.6 (2.0)	−24.1 (2.0)	14.5 (0.2)	1.6 (0.8)	−42 (10)
G35.04−0.50 MC2		−31.4 (2.0)	43.4 (0.3)	2.8 (0.7)	−94 (20)
G35.04−0.50 MC3		−36.0 (2.0)	49.9 (0.3)	5.4 (0.8)	−208 (30)
G35.04−0.50 MC4		−24.7 (2.0)	89.7 (0.3)	2.7 (0.6)	−70 (10)
G35.47+0.14 MC1	231.2 (2.2)	−31.4 (2.2)	14.3 (0.1)	3.5 (0.2)	−117 (10)
G35.47+0.14 MC2		−14.8 (2.2)	28.6 (0.1)	1.4 (0.3)	−23 (<10)
G35.47+0.14 MC3		−6.8 (2.2)	57.2 (0.1)	5.2 (1.6)	−37 (10)
G35.47+0.14 MC4		−80.4 (2.2)	77.9 (<0.1)	4.1 (0.1)	−350 (10)
G35.58−0.03 MC1	468.1 (1.4)	−19.4 (1.4)	12.5 (0.3)	2.0 (0.7)	−42 (10)
G35.58−0.03 MC2		−16.8 (1.4)	29.3 (0.3)	1.1 (0.7)	−19 (10)
G35.58−0.03 MC3		−50.9 (1.4)	52.2 (0.2)	5.4 (0.5)	−291 (20)
G35.58−0.03 MC4		−4.7 (1.4)	71.4 (1.7)	1.9 (3.7)	−10 (20)
G35.67−0.04 MC1	401.5 (2.0)	−21.4 (2.0)	13.6 (0.2)	1.2 (0.7)	−27 (10)
G35.67−0.04 MC2		−81.1 (2.0)	29.1 (0.1)	1.1 (0.1)	−98 (10)
G35.67−0.04 MC3		−28.5 (2.0)	61.5 (0.3)	3.3 (0.8)	−102 (20)
G36.40+0.02 MC1	84.3 (1.9)	−7.1 (1.9)	52.5 (0.2)	2.0 (0.6)	−15 (<10)
G36.40+0.02 MC2		−11.5 (1.9)	57.9 (0.2)	4.3 (0.5)	−52 (10)
G37.20−0.43 MC1	125.6 (1.5)	−13.0 (1.5)	36.0 (0.1)	2.4 (0.3)	−34 (<10)
G37.20−0.43 MC2		−8.0 (1.5)	79.9 (0.2)	2.6 (0.4)	−22 (<10)
G37.37−0.24 MC1	261.4 (2.1)	−27.8 (2.1)	40.1 (0.3)	4.8 (0.7)	−141 (20)
G37.37−0.24 MC2		−33.1 (2.1)	81.4 (0.2)	5.4 (0.6)	−191 (20)
G37.54−0.11 MC1	780.4 (1.8)	−38.7 (1.8)	19.3 (0.4)	2.5 (0.9)	−102 (30)
G37.54−0.11 MC2		−8.5 (1.8)	52.2 (2.5)	4.2 (6.5)	−38 (40)
G37.54−0.11 MC3		−20.6 (1.8)	66.5 (1.6)	10.3 (4.7)	−227 (70)
G37.54−0.11 MC4		−60.2 (1.8)	85.0 (0.3)	4.3 (0.9)	−274 (40)
G37.75−0.10 MC1	370.9 (2.0)	−20.9 (2.0)	14.6 (0.4)	1.3 (0.8)	−30 (20)
G37.75−0.10 MC2		−38.3 (2.0)	18.6 (0.3)	4.2 (0.8)	−172 (30)
G37.75−0.10 MC3		−12.7 (2.0)	45.8 (1.0)	3.0 (2.4)	−41 (30)
G37.75−0.10 MC4		−70.1 (2.0)	63.9 (0.1)	2.5 (0.3)	−186 (20)
G37.75−0.10 MC5		−61.0 (2.0)	85.9 (0.2)	4.7 (0.6)	−306 (30)
G37.76−0.20 MC1	1223.1 (2.5)	−86.9 (2.5)	13.6 (0.1)	2.3 (0.3)	−213 (20)
G37.76−0.20 MC2		−82.2 (2.5)	20.0 (0.1)	2.1 (0.2)	−184 (10)
G37.76−0.20 MC3		−17.2 (2.5)	38.1 (2.8)	1.9 (8.4)	−34 (80)
G37.76−0.20 MC4		−469.0 (2.5)	63.8 (<0.1)	5.5 (0.1)	−2740 (20)
G37.76−0.20 MC5		−48.2 (2.5)	83.1 (0.2)	4.3 (0.4)	−219 (20)
G37.76−0.20 MC6		−35.4 (2.5)	90.7 (0.2)	2.9 (0.5)	−108 (20)
G39.25−0.07 MC1	682.9 (1.9)	−9.6 (1.9)	−33.4 (0.8)	2.1 (2.1)	−22 (20)

TABLE 3—*Continued*

Source Direction[a]	S_c (mJy)	S_{H_2CO} (mJy)	V_{LSR} (km s^{-1})	FWHM (km s^{-1})	$\int S_v\,dv$ (mJy km s^{-1})
G39.25−0.07 MC2.....		−14.0 (1.9)	15.0 (0.7)	4.1 (2.5)	−61 (30)
G39.25−0.07 MC3.....		−29.1 (1.9)	22.0 (0.3)	4.0 (0.9)	−124 (20)
G39.25−0.07 MC4.....		−29.7 (1.9)	79.5 (0.3)	3.5 (0.9)	−112 (20)
G39.39−0.14 MC1.....	44.0 (1.0)	−6.9 (1.0)	16.8 (0.2)	1.8 (0.5)	−13 (<10)
G39.39−0.14 MC2.....		−6.2 (1.0)	30.3 (0.2)	2.4 (0.5)	−16 (<10)
G39.39−0.14 MC3.....		−4.7 (1.0)	41.4 (0.3)	2.5 (0.6)	−13 (<10)
G39.39−0.14 MC4.....		−6.1 (1.0)	52.8 (0.4)	4.2 (1.0)	−27 (<10)
G39.39−0.14 MC5.....		−40.1 (1.0)	66.5 (<0.1)	2.6 (0.1)	−112 (<10)
G39.39−0.14 MC6.....		−5.1 (1.0)	78.2 (0.3)	2.4 (1.0)	−14 (10)
G40.42+0.70 MC1.....	68.0 (1.4)	−29.4 (1.4)	12.3 (0.1)	4.7 (0.2)	−146 (10)
G40.42+0.70 MC2.....		−5.0 (1.4)	34.3 (0.6)	6.1 (1.6)	−33 (10)
G40.62−0.14 MC1.....	−47.3 (1.7)	−37.3 (1.7)	32.7 (0.1)	5.2 (0.2)	−207 (10)
G42.11−0.44 MC1.....	199.4 (1.7)	−17.6 (1.7)	55.5 (0.1)	3.7 (0.4)	−70 (10)
G42.11−0.44 MC2.....		−22.8 (1.7)	66.9 (0.1)	4.8 (0.3)	−116 (10)
G42.43−0.26 MC1.....	572.3 (2.0)	−21.4 (2.0)	10.1 (0.3)	1.4 (0.6)	−33 (10)
G42.43−0.26 MC2.....		−36.7 (2.0)	30.6 (0.2)	2.0 (0.5)	−79 (20)
G42.43−0.26 MC3.....		−13.3 (2.0)	35.3 (0.8)	3.9 (1.9)	−55 (20)
G42.43−0.26 MC4.....		−30.7 (2.0)	62.9 (0.4)	5.0 (0.9)	−163 (30)
G43.17+0.00 MC1.....	14308.4 (9.7)	−1890.0 (9.7)	12.5 (0.1)	11.0 (0.1)	−22100 (260)
G43.17+0.00 MC2.....		−801.0 (9.7)	39.5 (0.1)	1.8 (0.2)	−1500 (110)
G43.17+0.00 MC3.....		−972.0 (9.7)	62.9 (0.1)	2.4 (0.2)	−2450 (140)
G43.18−0.52 MC1.....	519.7 (2.0)	−63.7 (2.0)	56.7 (0.3)	4.7 (0.7)	−320 (40)
G43.18−0.52 MC2.....		−48.8 (2.0)	62.9 (0.3)	2.7 (0.8)	−140 (30)
G43.24−0.05 MC1.....	805.3 (2.1)	−304.0 (2.1)	9.2 (0.1)	6.2 (0.1)	−2000 (30)
G43.24−0.05 MC2.....		−32.2 (2.1)	38.9 (0.3)	2.5 (0.9)	−84 (20)
G43.24−0.05 MC3.....		−27.9 (2.1)	45.6 (0.3)	2.8 (1.1)	−83 (20)
G43.24−0.05 MC4.....		−16.7 (2.1)	50.9 (0.6)	1.9 (1.7)	−34 (20)
G43.24−0.05 MC5.....		−22.7 (2.1)	55.3 (0.5)	3.6 (1.5)	−87 (30)
G43.26−0.21 MC1.....	1676.6 (1.8)	−26.2 (1.8)	17.2 (0.3)	2.1 (0.6)	−60 (10)
G43.26−0.21 MC2.....		−209.0 (1.8)	40.4 (<0.1)	3.1 (0.1)	−686 (20)
G43.26−0.21 MC3.....		−86.3 (1.8)	58.1 (0.1)	1.9 (0.2)	−174 (20)
G43.26−0.21 MC4.....		−118.0 (1.8)	61.2 (0.1)	2.1 (0.2)	−257 (30)
G43.26−0.21 MC5.....		−50.6 (1.8)	65.9 (0.3)	5.3 (0.9)	−287 (30)
G43.79−0.12 MC1.....	109.7 (1.3)	−35.0 (1.3)	43.2 (0.1)	4.3 (0.1)	−159 (<10)
G43.79−0.12 MC2.....		−8.2 (1.3)	60.5 (0.1)	2.1 (0.3)	−19 (<10)
G45.48+0.18 MC1.....	1365.8 (2.2)	−230.0 (2.2)	60.0 (<0.1)	3.9 (<0.1)	−948 (<10)
G45.48+0.18 MC2.....		−48.8 (2.2)	66.5 (<0.1)	1.1 (0.9)	−55 (<10)
G45.82−0.29 MC1.....	435.4 (1.2)	−11.6 (1.2)	28.2 (0.8)	2.0 (0.8)	−24 (10)
G45.82−0.29 MC2.....		−34.5 (1.2)	54.6 (0.8)	7.6 (0.8)	−279 (10)
G45.82−0.29 MC3.....		−29.0 (1.2)	59.3 (0.8)	3.8 (0.8)	−117 (10)
G45.93−0.40 MC1.....	115.8 (1.8)	−29.5 (1.8)	61.0 (0.1)	4.2 (0.2)	−130 (10)
G48.63+0.23 MC1.....	233.0 (1.9)	−45.9 (1.9)	10.6 (0.1)	7.3 (0.1)	−355 (10)
G48.63+0.23 MC2.....		−13.9 (1.9)	51.0 (0.1)	1.5 (0.2)	−23 (<10)
G49.21−0.35 MC1.....	3423.1 (3.1)	−63.9 (3.1)	6.1 (0.1)	2.2 (0.1)	−152 (10)
G49.21−0.35 MC2.....		−208.0 (3.1)	62.1 (<0.1)	2.8 (0.1)	−610 (10)
G49.21−0.35 MC3.....		−777.0 (3.1)	65.9 (<0.1)	2.6 (<0.1)	−2140 (10)
G49.67−0.45 MC1.....	77.3 (1.2)	−25.1 (1.2)	69.2 (0.1)	3.9 (0.2)	−105 (<10)
G50.28−0.39 MC1.....	275.4 (1.8)	−27.0 (1.8)	39.8 (0.4)	4.6 (1.1)	−133 (20)
G50.28−0.39 MC2.....		−8.2 (1.8)	65.0 (1.4)	4.6 (3.2)	−40 (20)
G50.31+0.67 MC1.....	173.0 (1.7)	−10.2 (1.7)	25.8 (0.2)	4.7 (0.6)	−51 (10)
G51.68+0.72 MC1.....	−8.6 (2.0)	−26.7 (2.0)	2.6 (0.1)	7.8 (0.3)	−222 (10)
G52.23+0.74 MC1.....	240.2 (2.0)	−14.3 (2.0)	4.9 (0.2)	5.1 (0.5)	−77 (<10)
G52.23+0.74 MC2.....		−6.3 (2.0)	20.0 (0.3)	2.6 (1.0)	−17 (<10)
G52.23+0.74 MC3.....		−4.5 (2.0)	25.0 (0.6)	4.4 (1.8)	−21 (<10)
G53.03+0.12 MC1.....	27.7 (2.0)	−15.7 (2.0)	5.5 (0.4)	4.3 (1.0)	−72 (10)
G53.03+0.12 MC2.....		−10.9 (2.0)	21.5 (0.3)	1.5 (0.6)	−17 (10)
G53.03+0.12 MC3.....		−13.4 (2.0)	42.6 (0.3)	2.3 (0.9)	−33 (10)
G53.63+0.02 MC1.....	46.1 (1.0)	−22.6 (1.0)	24.2 (0.3)	2.5 (0.7)	−59 (20)
G54.09−0.06 MC1.....	341.9 (1.3)	−5.6 (1.3)	23.0 (2.2)	4.2 (8.0)	−25 (30)
G54.09−0.06 MC2.....		−38.5 (1.3)	40.5 (0.3)	4.6 (0.7)	−189 (30)
G54.09−0.06 MC3.....		−6.4 (1.3)	47.7 (1.2)	2.1 (2.6)	−14 (20)
G57.55−0.27 MC1.....	243.6 (1.1)	−8.1 (1.1)	2.0 (0.2)	6.5 (0.5)	−56 (<10)
G57.55−0.27 MC2.....		−5.2 (1.1)	10.4 (0.2)	1.9 (0.5)	−10 (<10)
G57.55−0.27 MC3.....		−6.2 (1.1)	31.1 (0.2)	1.9 (0.5)	−13 (<10)
G58.77+0.65 MC1.....	46.2 (1.2)	−35.2 (1.2)	32.5 (<0.1)	3.0 (0.1)	−112 (<10)

TABLE 3—*Continued*

Source Direction[a]	S_c (mJy)	S_{H_2CO} (mJy)	V_{LSR} (km s^{-1})	FWHM (km s^{-1})	$\int S_v\,dv$ (mJy km s^{-1})
G59.14−0.11 MC1	8.8 (1.8)	−13.9 (1.8)	26.4 (0.1)	3.1 (0.3)	−46 (<10)
G59.14−0.11 MC2		−6.8 (1.8)	61.2 (0.2)	1.4 (0.5)	−10 (<10)
G59.36−0.21 MC1	30.9 (1.1)	−17.5 (1.1)	29.2 (0.1)	3.5 (0.2)	−64 (<10)
G59.60+0.92 MC1	50.2 (0.4)	−24.0 (0.4)	37.3 (0.1)	4.0 (0.2)	−102 (<10)
G59.76−0.03 MC1	13.4 (1.7)	−25.4 (1.7)	20.9 (0.1)	2.8 (0.2)	−76 (<10)
G59.78+0.06 MC1	3.4 (1.7)	−19.0 (1.7)	22.6 (0.1)	4.7 (0.3)	−96 (10)
G63.05−0.34 MC1	0.042 (0.002)	...	...	...	...
G63.12+0.44	214.1 (1.8)	−14.4 (1.8)	21.4 (0.2)	5.4 (0.6)	−82 (10)
G69.54−0.98	36.8 (2.0)	−95.9 (2.0)	10.4 (0.0)	5.2 (0.1)	−530 (10)

NOTE.—Table 3 is also available in machine-readable form in the electronic edition of the *Astrophysical Journal*.

[a] Indicates the direction of the H_2CO cloud, but we do not imply an association between the H_2CO cloud and the UC H II region.

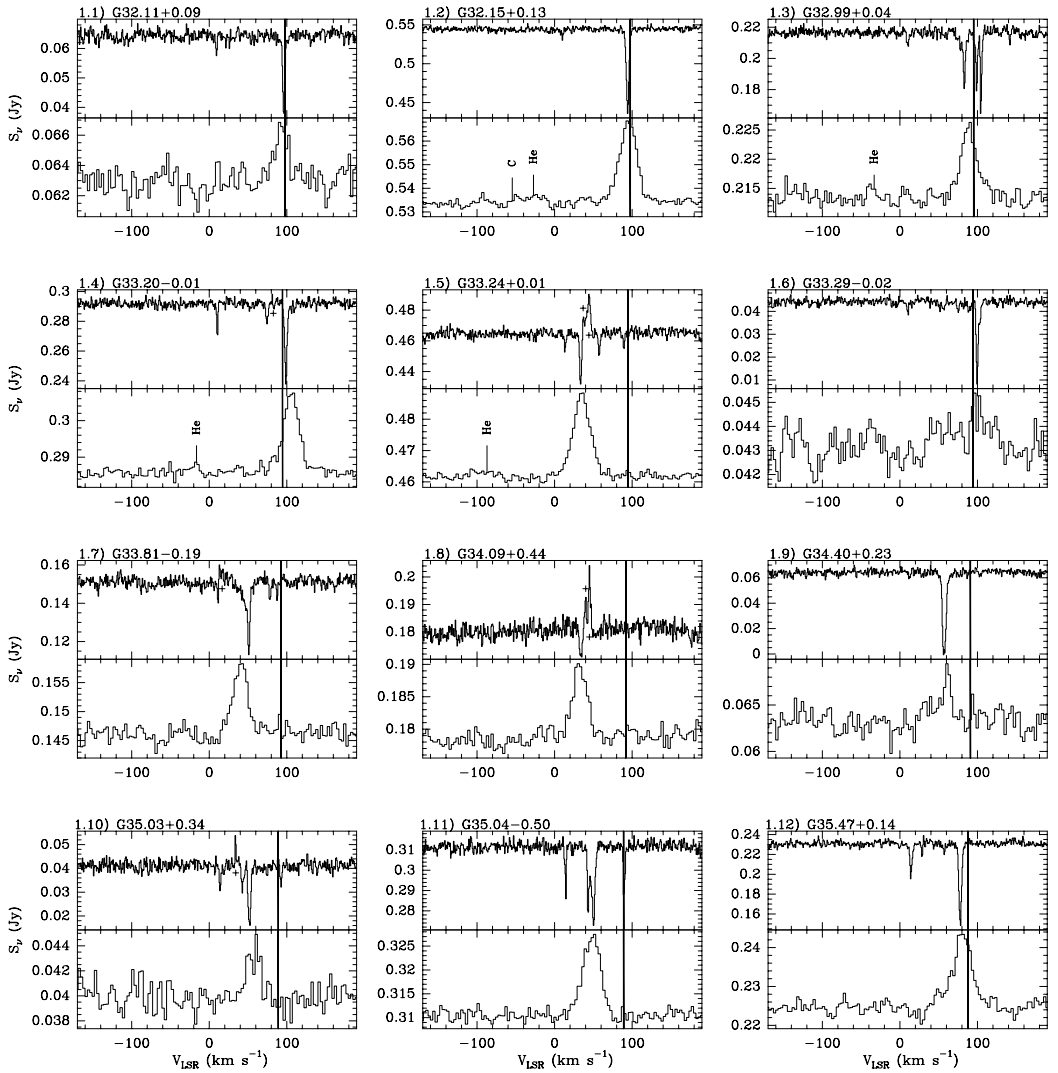

FIG. 1.—Spectra of H_2CO (*upper panel*) and H110α (*lower panel*) observed toward UC H II regions. The solid line indicates the tangent point velocity. Absorption in the off position is indicated by a plus sign. He and Ca recombination lines are indicated when detected.

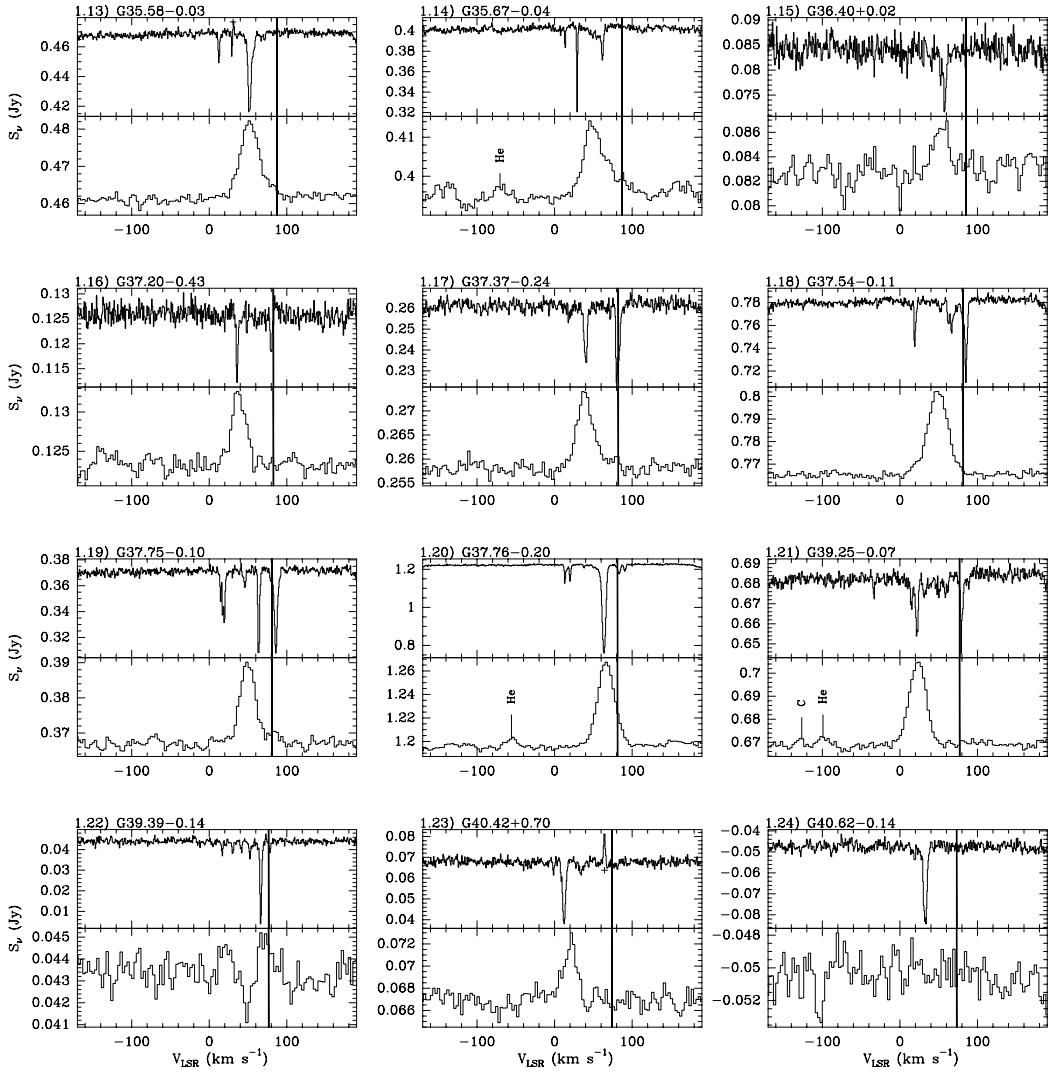

FIG. 1.—*Continued*

the following assumptions: (1) the Galaxy rotates according to the model of Brand & Blitz (1993), (2) clouds detectable in H_2CO are common in the disk and are present between us and UC H II regions at the far distance, and (3) only one H II region is located within the beam. UC H II regions are not classified owing to peculiar motions if the H110α line velocity is within 10 km s^{-1} of or greater than the tangent velocity (see Fig. 2). For UC H II regions that are classified, the H_2CO spectrum was examined for absorption lines between the source velocity plus 10 km s^{-1} (to account for peculiar motions) and the tangent velocity plus 10 km s^{-1}. If H_2CO absorption was found in this region, the UC H II region was classified at the far distance. If no H_2CO absorption was found, the near distance was adopted. The clouds detected in H_2CO absorption against the UC H II regions were also classified when possible. Those molecular clouds with detectable H_2CO absorption at lower velocities than the H110α line -10 km s^{-1} are unambiguously at the near distance, the far distance being behind the UC H II region and incapable of permitting absorption against the UC H II region. H_2CO clouds with higher velocities than $V_{H110\alpha}+10$ km s^{-1} (but lower than the tangent point velocity) still suffer from the distance ambiguity because both the near and far positions are in front of the UC H II region. In Table 4 we report the kinematic distances of 26 UC H II regions and 72 intervening clouds for the cases that are unambiguous.

Five sources were at the near distance, and 21 were at the far distance. Any source with an H110α velocity greater than tangent velocity was not classified, although we report the distance as the tangent distance. Seven sources were in this category. Finally, 11 UC H II regions had velocities between the tangent velocity and the tangent velocity minus 10 km s^{-1}. These sources are particularly difficult to classify owing to peculiar motions. We do not classify or give a distance to these sources. A mean of 1.6, 2.1, and 3.1 clouds were observed toward UC H II regions at the near, tangent, and far positions, respectively. Distance errors are calculated by propagating an assumed peculiar velocity of 10 km s^{-1}.

When an UC H II region at the far kinematic distance has no intervening cloud detectable in H_2CO at a higher velocity than the H110α line, the above method will mistakenly place the UC H II region at the near kinematic distance. To determine the likelihood of this error, we have estimated the frequency of clouds detectable in H_2CO within a 1′ cone through the inner Galaxy. On the basis of the average

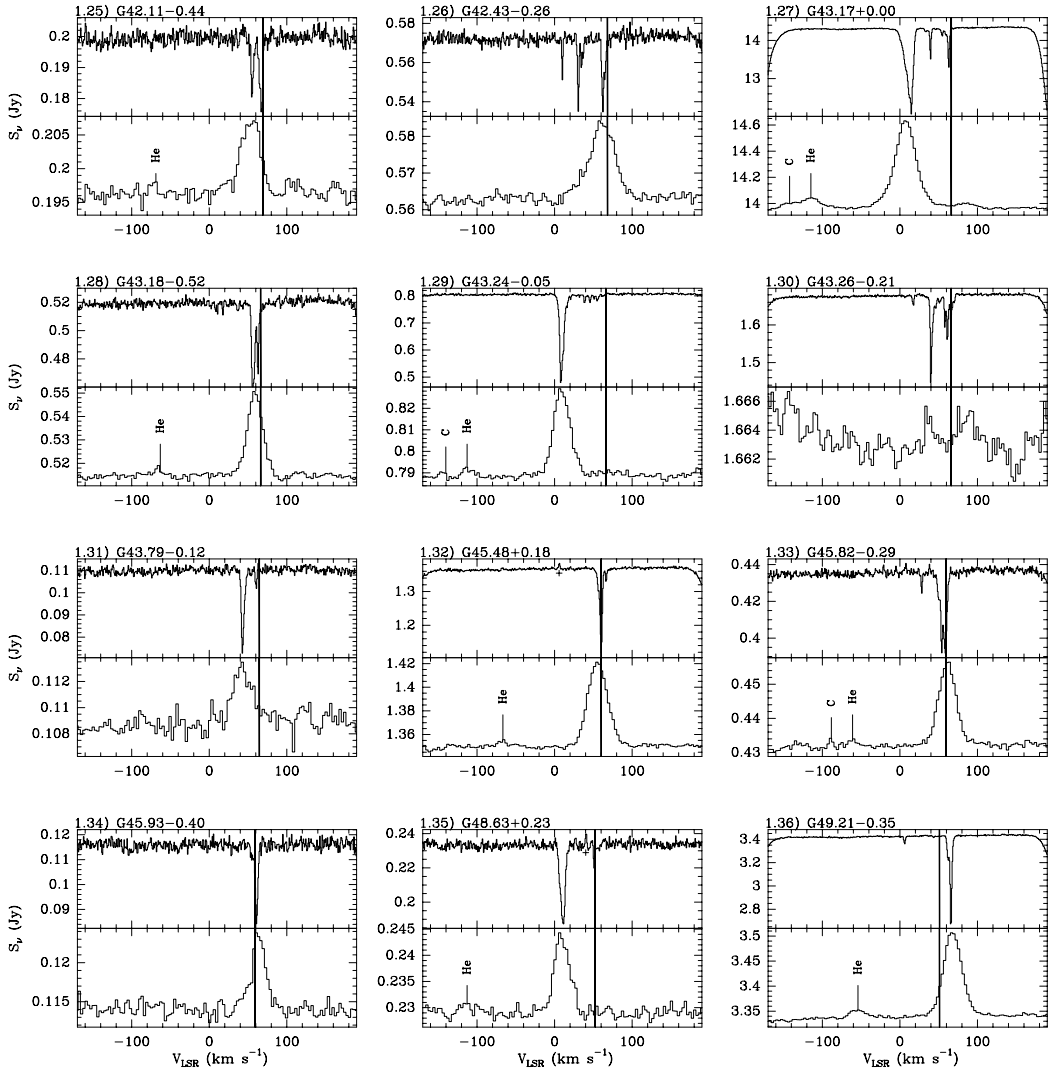

FIG. 1.—*Continued*

number of all clouds detected in H_2CO toward classified UC H II regions (see below) in this study, we calculate a cloud frequency of one cloud per 2.9 kpc. Clouds detectable in H_2CO are undoubtedly not distributed uniformly in the galactic disk. However, this estimate suggests that a lack of clouds detectable in H_2CO may be a problem when the difference between the near and far distances is small (i.e., <2.9 kpc).

A second cause of misclassification is possible when an UC H II region at the near distance is in front of a cloud containing H_2CO with $v_{H_2CO} > v_{H110\alpha}$. The cloud containing H_2CO may absorb the cosmic microwave background radiation (CMBR), creating an absorption feature at a velocity higher than the UC H II region. First detected by Palmer et al. (1969) and designated anomalous absorption, this phenomenon would cause an UC H II region to be misclassified at the far distance. Since we detect only seven absorption features in off-source integrations (compared to 134 in on-source integrations), we conclude that this effect is rare and not a significant source of error.

We share one common source with Araya et al. (2002) and Fish et al. (2003), G35.58−0.03. Araya et al. (2002) reported a near distance, whereas Fish et al. (2003) reported a far distance. We obtained deeper observations than Araya et al. (2002) for the purpose of resolving this disagreement. We agree with Fish et al. (2003) on a far distance. We share 13 sources with Kuchar & Bania (1994), who observed H I toward UC H II regions using the Arecibo Telescope with a $3'$ beam. Of these, we agree on the near-far distance resolution for nine sources, disagree on none, and are uncertain about four (G32.15+0.13, G42.43−0.26, G45.82−0.29, and G54.09−0.06). On the basis of our criteria, we do not classify any of these four because they have velocities near the tangent velocity. Kuchar & Bania (1994) classify them strictly to the near or far distance. These differences, however, are within our quoted distance errors. Kolpak et al. (2002) resolved the kinematic distance ambiguity toward 49 UC H II regions by observing H I in absorption with the VLA. We share 10 sources with Kolpak et al. (2002), of which we agree on seven, disagree on none, and have uncertain comparisons on three (G42.43−0.26, G43.18−0.52, and G45.82−0.29). The uncertain comparisons are caused by the difficultly in classifying sources with velocity within 10 km s^{-1} of the tangent velocity. Furthermore, all sources on which we have uncertain comparisons with Kolpak et al. (2002) have $D_{far} - D_{near} \lesssim 3$ kpc. While observations of

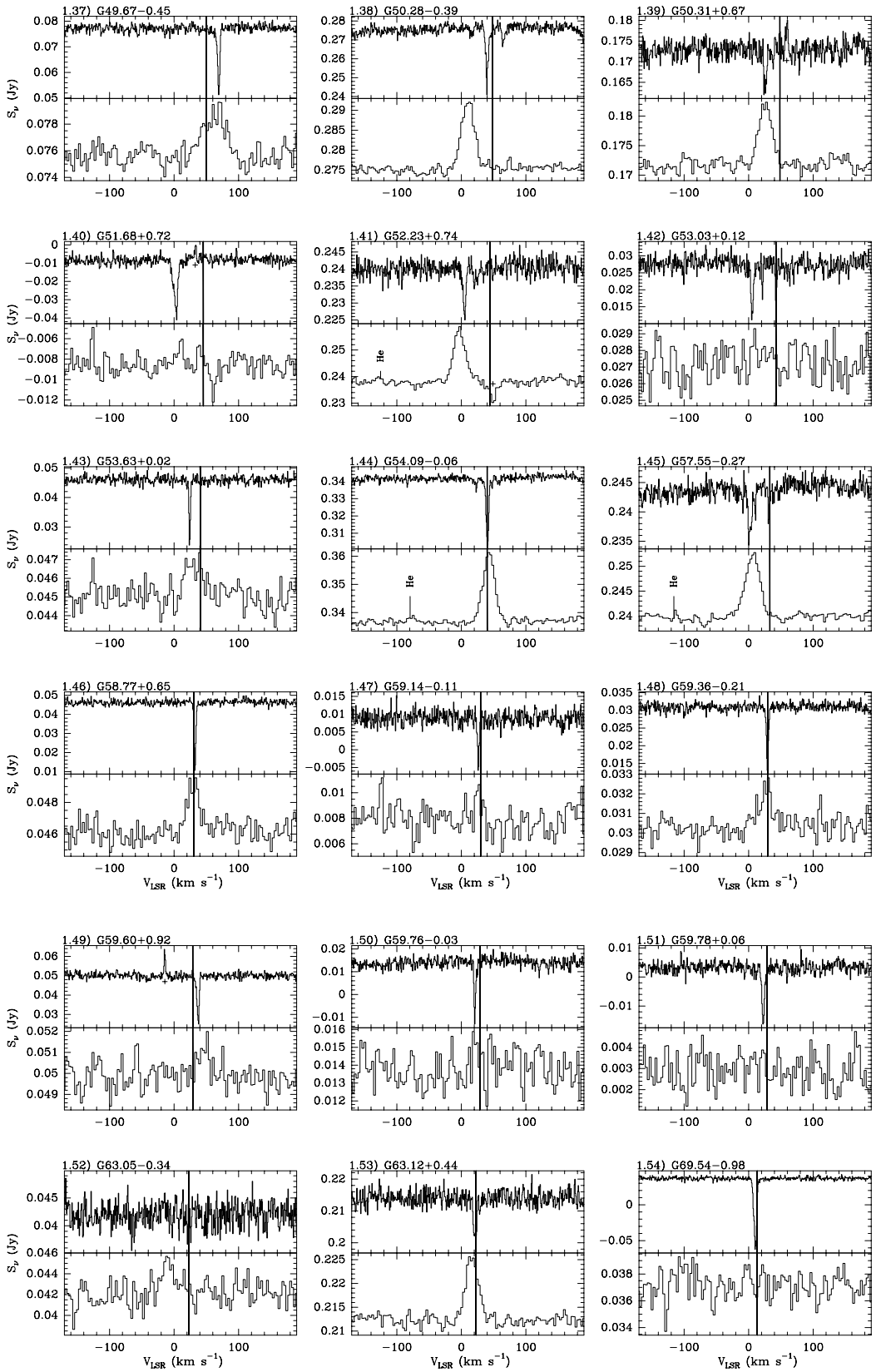

FIG. 1.—*Continued*

TABLE 4

KINEMATIC PARAMETERS

Source	V_{LSR} (km s^{-1})	D_{near} (kpc)	D_{far} (kpc)	V_{TP} (km s^{-1})	D_{TP} (kpc)	D_{LSR} (kpc)	z (pc)	D_{GC} (kpc)	Near/Far
G32.11+0.09.....	93.0 (1.5)	6.2	8.2	97.8	7.2	...	...	4.62	...[a]
MC1	9.3 (0.2)	0.8	13.6	97.8	7.2	$0.784^{+0.7}_{-0.8}$	1	7.85	Near
G32.15+0.13.....	95.0 (0.2)	6.5	7.9	97.7	7.2	...	...	4.58	...[a]
MC1	10.3 (0.5)	0.9	13.5	97.7	7.2	$0.860^{+0.7}_{-0.8}$	2	7.79	Near
G32.99+0.04.....	89.0 (0.6)	6.0	8.3	95.1	7.1	...	...	4.77	...[a]
MC1	10.3 (0.5)	0.8	13.4	95.1	7.1	$0.847^{+0.7}_{-0.8}$	1	7.80	Near
MC4	104.6 (0.1)	...	...	95.1	7.1	$7.130^{+1.5}_{-1.5}$	5	4.43	...[b]
MC5	141.8 (0.4)	...	...	95.1	7.1	$7.130^{+1.5}_{-1.5}$	5	3.77	...[b]
G33.20−0.01.....	105.8 (0.3)	...	...	94.5	7.1	$7.1^{+1.5}_{-1.5}$	−1	4.41	...[b]
MC1	10.5 (0.1)	0.9	13.4	94.5	7.1	$0.863^{+0.7}_{-0.8}$	0	7.79	Near
MC2	74.5 (0.2)	4.9	9.3	94.5	7.1	$4.903^{+0.7}_{-0.6}$	−1	5.15	Near
G33.24+0.01.....	35.1 (0.3)	2.6	11.7	94.4	7.1	$11.7^{+0.6}_{-0.6}$	2	6.52	Far
MC1	13.6 (0.8)	1.1	13.1	94.4	7.1	$1.100^{+0.7}_{-0.8}$	0	7.60	Near
MC4	89.4 (0.7)	6.1	8.2	94.4	7.1	...	...	4.77	...[a]
G33.81−0.19.....	40.3 (0.6)	2.9	11.3	92.7	7.1	$11.3^{+0.6}_{-0.6}$	−37	6.32	Far
MC1	11.3 (0.1)	0.9	13.2	92.7	7.1	$0.919^{+0.7}_{-0.8}$	−3	7.75	Near
MC4	87.6 (0.2)	6.0	8.1	92.7	7.1	...	...	4.85	...[a]
G34.09+0.44.....	32.6 (0.5)	2.4	11.7	91.9	7.0	$2.4^{+0.6}_{-0.7}$	18	6.66	Near
G34.40+0.23.....	60.1 (1.3)	4.1	10.0	90.9	7.0	$4.1^{+0.6}_{-0.6}$	16	5.64	Near
G35.03+0.34.....	57.2 (1.4)	3.9	10.0	89.1	7.0	$10.0^{+0.6}_{-0.6}$	59	5.76	Far
MC1	14.1 (0.2)	1.1	12.8	89.1	7.0	$1.113^{+0.7}_{-0.8}$	7	7.62	Near
MC2	43.1 (0.2)	3.0	10.9	89.1	7.0	$3.031^{+0.6}_{-0.6}$	18	6.26	Near
MC4	92.6 (0.2)	...	...	89.1	7.0	$6.960^{+1.6}_{-1.6}$	41	4.80	...[b]
G35.04−0.50.....	48.0 (0.4)	3.3	10.6	89.1	7.0	$10.6^{+0.6}_{-0.6}$	−92	6.08	Far
MC1	14.5 (0.2)	1.1	12.8	89.1	7.0	$1.143^{+0.7}_{-0.8}$	−10	7.59	Near
MC4	89.7 (0.3)	...	...	89.1	7.0	$6.959^{+1.6}_{-1.6}$	−61	4.87	...[b]
G35.47+0.14.....	80.9 (0.5)	5.6	8.2	87.8	6.9	...	...	5.10	...[a]
MC1	14.3 (0.1)	1.1	12.7	87.8	6.9	$1.129^{+0.7}_{-0.8}$	3	7.61	Near
MC2	28.6 (0.1)	2.1	11.7	87.8	6.9	$2.114^{+0.6}_{-0.7}$	5	6.89	Near
MC3	57.2 (0.1)	3.9	9.9	87.8	6.9	$3.902^{+0.6}_{-0.6}$	10	5.78	Near
G35.58−0.03[c].....	52.5 (0.3)	3.6	10.2	87.5	6.9	$10.2^{+0.6}_{-0.6}$	−5	5.95	Far
MC1	12.5 (0.3)	1.0	12.8	87.5	6.9	$0.995^{+0.7}_{-0.8}$	−1	7.71	Near
MC2	29.3 (0.3)	2.2	11.7	87.5	6.9	$2.157^{+0.6}_{-0.7}$	−1	6.86	Near
G35.67−0.04.....	51.9 (0.7)	3.6	10.2	87.2	6.9	3.6 ± 0.6	−2	5.97	Near
MC1	13.6 (0.2)	1.1	12.7	87.2	6.9	$1.075^{+0.7}_{-0.8}$	−1	7.65	Near
MC2	29.1 (0.1)	2.1	11.7	87.2	6.9	$2.146^{+0.6}_{-0.7}$	−1	6.87	Near
G36.40+0.02.....	53.3 (1.4)	3.7	10.0	85.1	6.8	$3.7^{+0.7}_{-0.6}$	1	5.95	Near
G37.20−0.43.....	38.0 (0.5)	2.7	10.8	82.8	6.8	$10.8^{+0.7}_{-0.6}$	−81	6.54	Far
MC2	79.9 (0.2)	5.9	7.6	82.8	6.8	...	...	5.21	...[a]
G37.37−0.24.....	39.4 (0.4)	2.8	10.7	82.3	6.8	$10.7^{+0.7}_{-0.6}$	−45	6.50	Far
MC2	81.4 (0.2)	6.3	7.2	82.3	6.8	...	...	5.18	...[a]
G37.54−0.11.....	48.9 (0.2)	3.4	10.1	81.8	6.7	$10.1^{+0.6}_{-0.7}$	−19	6.15	Far
MC1	19.3 (0.4)	1.5	12.0	81.8	6.7	1.470 ± 0.7	−3	7.39	Near
MC4	85.0 (0.3)	...	...	81.8	6.7	6.740 ± 1.7	−13	5.10	...[b]
G37.75−0.10.....	49.7 (0.3)	3.5	10.0	81.2	6.7	$10.0^{+0.6}_{-0.7}$	−17	6.13	Far
MC1	14.6 (0.4)	1.1	12.3	81.2	6.7	$1.130^{+0.7}_{-0.8}$	−2	7.64	Near
MC2	18.6 (0.3)	1.4	12.0	81.2	6.7	1.421 ± 0.7	−2	7.43	Near
MC5	85.9 (0.2)	...	...	81.2	6.7	6.721 ± 1.7	−12	5.09	...[b]
G37.76−0.20.....	66.6 (0.2)	4.7	8.8	81.2	6.7	$8.8^{+0.7}_{-0.9}$	−31	5.60	Far
MC1	13.6 (0.1)	1.1	12.4	81.2	6.7	$1.056^{+0.7}_{-0.8}$	−4	7.69	Near
MC2	20.0 (0.1)	1.5	11.9	81.2	6.7	1.515 ± 0.7	−5	7.36	Near
MC3	38.1 (2.8)	2.7	10.7	81.2	6.7	$2.724^{+0.6}_{-0.7}$	−10	6.56	Near
MC5	83.1 (0.2)	...	...	81.2	6.7	6.720 ± 1.7	−23	5.16	...[b]
MC6	90.7 (0.2)	...	...	81.2	6.7	6.720 ± 1.7	−23	4.98	...[b]
G39.25−0.07.....	23.0 (0.2)	1.7	11.4	77.0	6.6	11.4 ± 0.7	−14	7.25	Far
MC4	79.5 (0.3)	...	...	77.0	6.6	6.582 ± 1.7	−8	5.31	...[b]
G40.42+0.70.....	20.1 (0.8)	1.5	11.4	73.7	6.5	11.4 ± 0.7	140	7.41	Far
G42.11−0.44.....	53.4 (0.6)	4.0	8.7	69.1	6.3	$8.7^{+0.8}_{-1.0}$	−66	6.16	Far
MC2	66.9 (0.1)	5.5	7.1	69.1	6.3	...	...	5.76	...[a]
G42.43−0.26.....	61.5 (0.4)	4.8	7.8	68.3	6.3	...	...	5.93	...[a]
MC1	30.6 (0.2)	2.3	10.3	68.3	6.3	2.269 ± 0.7	−10	7.00	Near
MC2	35.3 (0.8)	2.6	9.9	68.3	6.3	2.603 ± 0.7	−12	6.81	Near
G43.17+0.00.....	7.4 (0.3)	0.6	11.8	66.3	6.2	$11.8^{+0.8}_{-0.7}$	0	8.09	Far
MC3	62.9 (0.1)	5.1	7.3	66.3	6.2	...	...	5.91	...[a]

TABLE 4—*Continued*

Source	V_{LSR} (km s^{-1})	D_{near} (kpc)	D_{far} (kpc)	V_{TP} (km s^{-1})	D_{TP} (kpc)	D_{LSR} (kpc)	z (pc)	D_{GC} (kpc)	Near/Far
G43.18−0.52.....	59.1 (0.2)	4.6	7.8	66.3	6.2	...	...	6.02	...[a]
G43.24−0.05.....	9.4 (0.2)	0.7	11.7	66.1	6.2	$11.7^{+0.8}_{-0.7}$	−10	7.98	Far
G43.79−0.12.....	43.3 (1.1)	3.3	9.0	64.7	6.1	$9.0^{+0.8}_{-0.9}$	−19	6.55	Far
MC2	60.5 (0.2)	4.9	7.3	64.7	6.1	...	...	6.00	...[a]
G45.48+0.18.....	55.6 (0.1)	4.7	7.3	60.3	6.0	...	...	6.20	...[a]
MC2	66.5 (0.0)	...	...	60.3	6.0	5.960 ± 1.9	19	5.88	...[b]
G45.82−0.29.....	61.2 (0.2)	...	...	59.4	5.9	5.9 ± 2.0	−30	6.05	...[b]
MC1	28.2 (0.8)	2.2	9.7	59.4	5.9	2.159 ± 0.8	−11	7.16	Near
G45.93−0.40.....	63.8 (0.5)	...	...	59.2	5.9	5.9 ± 2.0	−41	5.97	...[b]
G48.63+0.23.....	9.4 (0.4)	0.8	10.5	52.5	5.6	10.5 ± 0.8	42	8.02	Far
MC2	51.0 (0.1)	4.9	6.4	52.5	5.6	...	...	6.42	...[a]
G49.21−0.35.....	68.1 (0.2)	...	...	51.1	5.6	5.6 ± 2.1	−34	5.95	...[b]
MC1	6.1 (0.1)	0.5	10.6	51.1	5.6	0.491 ± 0.8	−3	8.19	Near
G49.67−0.45.....	62.7 (1.5)	...	...	50.0	5.5	5.5 ± 2.1	−43	6.11	...[b]
G50.28−0.39.....	10.3 (0.3)	0.8	10.0	48.6	5.4	10.0 ± 0.8	−68	7.99	Far
MC1	39.8 (0.4)	3.5	7.4	48.6	5.4	...	...	6.82	...[a]
MC2	65.0 (1.4)	...	...	48.6	5.4	5.432 ± 2.1	−37	6.06	...[b]
G50.31+0.67.....	25.9 (0.5)	2.1	8.7	48.5	5.4	$2.1^{+0.9}_{-0.8}$	25	7.33	Near
G52.23+0.74.....	−3.0 (0.4)	−0.2	10.7	44.1	5.2	$10.7^{+0.9}_{-0.8}$	138	8.65	Far
G53.63+0.02.....	31.2 (2.2)	2.9	7.2	41.0	5.0	...	...	7.18	...[a]
G54.09−0.06.....	42.8 (0.2)	...	...	40.0	5.0	5.0 ± 2.2	−5	6.79	...[b]
MC1	23.0 (2.2)	2.0	7.9	40.0	5.0	$2.029^{+1.1}_{-0.9}$	−2	7.49	Near
G57.55−0.27.....	6.3 (0.3)	0.6	8.6	32.9	4.6	$8.6^{+0.9}_{-1.0}$	−40	8.21	Far
MC3	31.1 (0.2)	3.6	5.5	32.9	4.6	...	...	7.24	...[a]
G58.77+0.65.....	30.0 (1.1)	3.9	4.9	30.5	4.4	...	...	7.29	...[a]
G59.36−0.21.....	26.6 (1.6)	3.1	5.6	29.4	4.3	...	...	7.41	...[a]
G59.60+0.92.....	46.8 (2.7)	...	...	29.0	4.3	4.3 ± 2.3	69	6.76	...[b]
G63.05−0.34.....	−9.3 (2.3)	−0.9	8.6	22.9	3.9	$8.6^{+0.9}_{-1.0}$	−51	8.94	Far
G63.12+0.44.....	16.4 (0.4)	1.9	5.7	22.8	3.8	...	...	7.82	...[a]

NOTE.—Table 4 is also available in machine-readable form in the electronic edition of the *Astrophysical Journal*.

[a] This source has a velocity within 10 km s^{-1} of the tangent velocity. Because we are unable to strongly distinguish between the near and far distance, we do not give a classification or distance.

[b] This source has a velocity higher then the tangent velocity. We locate this source at the tangent point, but this position should be taken with caution since its velocity is not strictly predicted in our rotation model.

[c] Araya et al. 2002 report the near kinematic distance to this source. The data presented here have a better S/N than the Araya et al. spectra. Our observations revealed a weak H_2CO absorption not detected by Araya et al. that implies the *far* kinematic distance.

H_2CO, compared to single-dish H I, have the advantage of higher spatial resolution, they suffer from the lower abundance and sparser distribution of H_2CO relative to H I. Also, as noted earlier, H_2CO (1_{10}–1_{11}) can absorb the CMBR. On the other hand, single-dish H I absorption observations require an emission profile in the absence of the background continuum source, which is approximated by averaging profiles from multiple positions near the continuum source. H I can also be self-absorbed. As we see from comparison of our results with Kuchar & Bania (1994) and Kolpak et al. (2002), both techniques generally agree on the near-far distance resolution, especially when $D_{far} - D_{near} > 3$ kpc. Cases of disagreement are frequently caused by a difference in measured source velocity or classification criteria. Rarely does the absence of clouds with detectable H_2CO between the near and far distances lead to a misclassification.

4. DISCUSSION

We show the galactic position of UC H II regions observed in this survey along with other comparable studies (Araya et al. 2002; Fish et al. 2003; Kolpak et al. 2002) in Figure 3 along with the spiral arm model of Georgelin & Georgelin (1976) as modified by Taylor & Cordes (1993). Segments of the Perseus and Sagittarius arms appear to be reasonably well populated by the UC H II regions, but the Scutum arm is not distinguishable and the Norma arm is not sampled well enough to comment on. There is too much spread in UC H II region positions to warrant a sophisticated analysis. The spread in positions is probably due to errors caused by departures from circular motion. The quoted distance errors are shown in Figure 4, along with the Taylor & Cordes (1993) model of the spiral arms. The distance errors are about the same as the separation between arms as portrayed in the Taylor & Cordes (1993) model; however, UC H II regions seem to be located preferentially along the
Perseus and Sagittarius arms. Interior to the Sagittarius arm a patten is not so obvious. The local spur is also apparent.

The clouds detectable in H_2CO that we classify (see Table 4) trace two principle galactic structures. The clouds associated with UC H II regions (based on similar velocities) trace the same spiral arms as the UC H II regions (see Fig. 3). Those clouds not associated with UC H II regions trace the local spur, although there is scatter sufficient to bridge the Sagittarius and Scutum arm. There are 24 clouds that have velocities greater than the tangent velocity. These velocities range from 0.3 to 46.6 km s^{-1} greater than the tangent

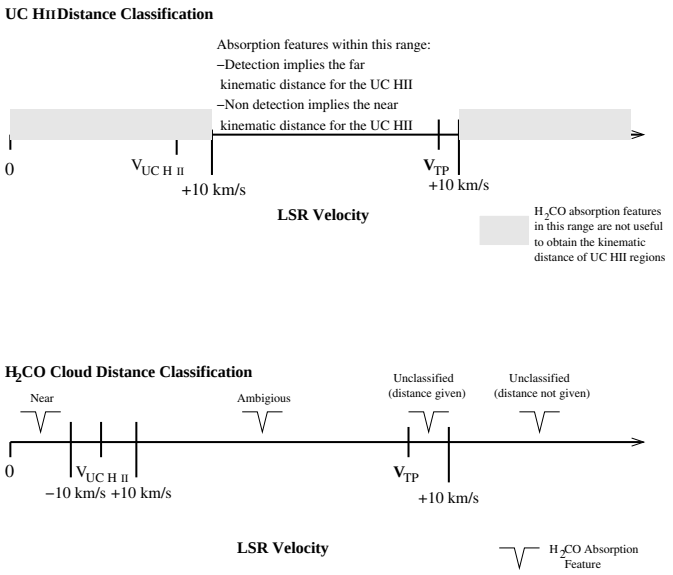

FIG. 2.—Criteria for resolution of distance ambiguity toward UC H II regions (*top panel*) and H_2CO clouds (*bottom panel*). If H_2CO absorption is observed in the velocity range indicated in the top panel, the UC H II region is classified at the far distance; otherwise, the UC H II region is classified at the near distance. For classifying H_2CO clouds, the bottom panel indicates which clouds are near, ambiguous, or near the tangent point and thus unclassified.

velocity with a mean of 9.0 km s^{-1} and median of 4.7 km s^{-1}. Thus, there appears to be a significant population of clouds detectable in H_2CO that have peculiar motions $\gtrsim 10$ km s^{-1}.

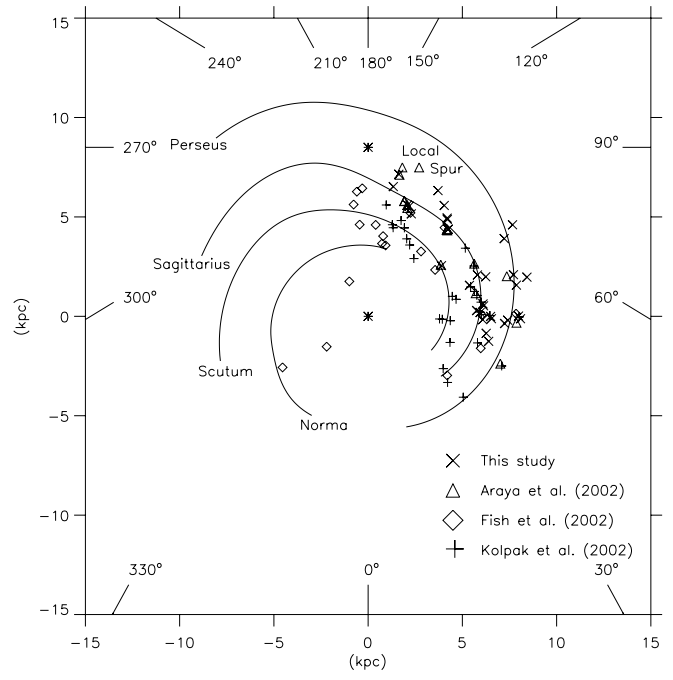

FIG. 3.—UC H II regions observed in this study (*crosses*), Araya et al. (2002, *triangles*) Kolpak et al. (2002, *plus signs*) and Fish et al. (2003, *diamonds*). We have included all UC H II region surveys that resolve the distance ambiguity and have resolution $\lesssim 1'$. The spiral arm model of Taylor & Cordes (1993) is indicated by solid lines. The solar position and Galactic center are indicated by stars.

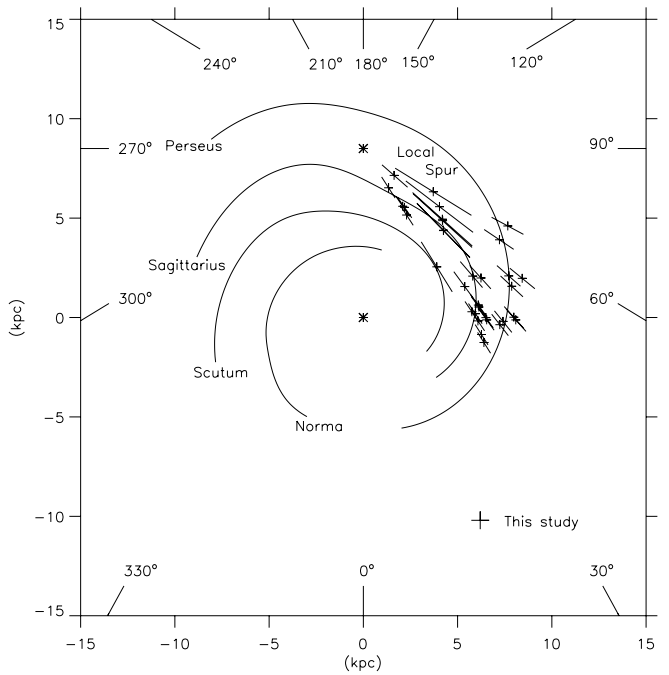

FIG. 4.—UC H II regions observed in this study (*plus sign*) with distance errors reported in Table 4. The spiral arm model of Georgelin & Georgelin (1976) and modified by Taylor & Cordes (1993) is indicated by solid lines. The solar position and Galactic center are indicated by stars.

The sample of UC H II regions in this study suffers severely from selection bias rendering any discussion of population scale height inappropriate. Fish et al. (2003) argue that Galactic latitude can be used to resolve the distance ambiguity. Specifically, Fish et al. (2003) suggest that UC H II regions should be classified as near or far based on which distance is closer to $d_{\rm pred} = 1.84|b|^{-1}$. This criterion agrees with the classification given here for 16 sources and disagrees for 10 sources and thus is not predictive for the sample presented here. A graphical way to visualize this is presented in Figure 5. From our data it is clear that no latitude-distance relationship holds for $|b| < 1^\circ$. It is also worth noting the lack of sources located in the far kinematic distance with $|b| > 3^\circ$ in the Fish et al. (2003) sample from which the latitude-distance criterion was derived. All the sources from Fish et al. (2003) within this range are close to the Galactic center ($|l| < 15^\circ$; see Fig. 3). The sample presented here has a wider distribution in longitude and thus reveals the weakness in the criterion of Fish et al. (2003).

5. CONCLUSIONS

Fifty-four UC H II regions located within the GLIMPSE survey region ($|b| \leq 1^\circ$ and $10^\circ < l < 70^\circ$) were observed simultaneously in the H_2CO and H110α lines. All UC H II regions showed absorption in H_2CO, indicating the well-known relationship between molecular clouds and star formation. By analyzing absorption in H_2CO, the distance ambiguity was resolved toward 44 UC H II regions (26 located at either the far or near distance, and 18 located near the tangent point). Since UC H II regions trace massive star formation regions, they should also closely trace Galactic spiral arms. In fact, the UC H II regions in our sample do appear to be preferentially located along the segments of the

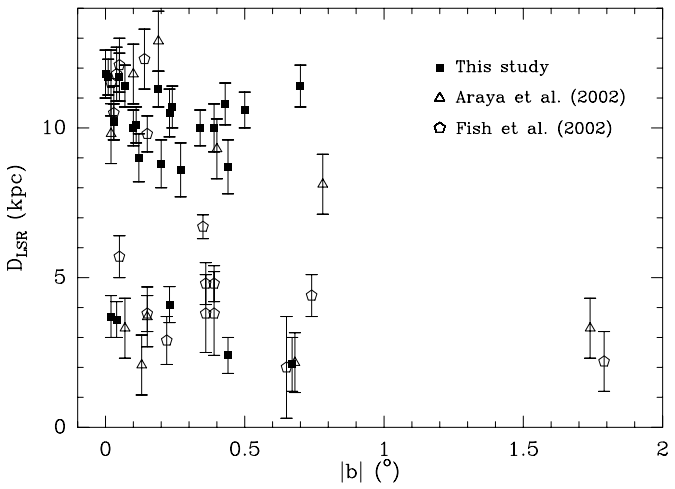

FIG. 5.—Kinematic distance to sources with resolved distance ambiguity, i.e., neither located at the tangent point nor with negative LSR velocities, as a function of Galactic latitude. The sources included in the plot are from our sample (*squares*), Araya et al. (2002, *triangles*) and Fish et al. (2003, *pentagons*). Note the far-distance population at $|b| > 0.^{\circ}3$ that is present in the Araya et al. (2002) sample as well as in our sample, but is absent in the Fish et al. (2003) data.

Perseus and Sagittarius arms (as delineated in Taylor & Cordes 1993). A correlation with the Scutum arm is less well defined. The local spur (see Fig. 3) is also traced by UC H II regions in agreement with Kurtz et al. (1994). We reiterate that distance errors (owing to departures from model velocities, possible absence of H_2CO between the near and far distances, and possible absorption of CMBR) are about the same as the separation of spiral arms. Thus, delineation of large-scale spiral arm structure using this technique is not yet a sharp enough tool to accurately determine the location of spiral arms.

Using Galactic latitude to resolve the distance ambiguity (Fish et al. 2003) was found not to be applicable to our sample. We estimate one molecular cloud detectable in H_2CO about every 2.9 kpc in the inner Galaxy, which suggests that sources near the tangent point (i.e., $D_{\rm far} - D_{\rm near} < 2.9$ kpc) could be erroneously classified at the near distance. In comparison to similar studies using H I, we find agreement on all 16 of the common sources within our quoted distance errors. Therefore, our data indicate that the kinematic distance determinations based on H_2CO–H110α measurements agree with the determination made using H I absorption for sources where the difference in the near and far distances is greater than 3 kpc.

We would like to acknowledge an anonymous referee whose comments improved the clarity of the paper, especially in § 3. We would also like to acknowledge Vincent Fish for his helpful comments. C. W. acknowledges partial support from the Wisconsin Space Grant Consortium. E. B. C. acknowledges partial support from NSF grant AST-9986548. P. H. acknowledges partial support from the Research Corporation award CC4996, as well as from NSF grant AST-0098524. S. K. acknowledges partial support from CONACYT grant 36568-E.

REFERENCES

Araya, E., Hofner, P., Churchwell, E., & Kurtz, S. 2002, ApJS, 138, 63
Bania, T. M., & Lockman, F. J. 1984, ApJS, 54, 513
Brand, J., & Blitz, L. 1993, A&A, 275, 67
Brogan, C. L., & Troland, T. H. 2001, ApJ, 550, 799
Fish, V. L., Reid, M. J., Wilner, D. J., & Churchwell, E. 2003, ApJ, in press
Georgelin, Y. M., & Georgelin, Y. P. 1976, A&A, 49, 57
Kolpak, M. A., Jackson, J. M., Bania, T. M., & Clemens, D. P. 2002, ApJ, 578, 868
Kuchar, T. A., & Bania, T. M. 1994, ApJ, 436, 117
Kurtz, S., Churchwell, E., & Wood, D. O. S. 1994, ApJS, 91, 659
Palmer, P., Zuckerman, B., Buhl, D., & Snyder, L. E. 1969, Astrophys. Lett., 156, 147
Taylor, J. H., & Cordes, J. M. 1993, ApJ, 411, 674
Vallee, J. P. 1995, ApJ, 454, 119
Wood, D. O. S., & Churchwell, E. 1989, ApJ, 340, 265